Memoirs of the Faculty of Engineering, Nagoya University
Vol. 38, No. 2 (1986) — Research Report —

# A THREE-DIMENSIONAL FLOW FIELD AROUND A TURBULENT JET INJECTED NORMALLY INTO A CONFINED CROSS FLOW

YOSHIYUKI SUGIYAMA, YOSHIO KOJIMA and FUMIO NIWA

*Department of Aeronautical Engineering*

(Received October 31, 1986)

**Abstract**

Results are reported of experiments on the characteristics of the flow field affected by a jet impinging on an opposite channel wall. Longitudinal and transverse distributions of velocity and also jet and vortex center-lines are presented. The present jet center-line lies along that of the unconfined jet, but the present vortex center-line deviates greatly from that of the unconfined jet. Flow patterns are considered on the upper and lower walls on the basis of flow visualization technique. Oil flow patterns reveal that there are two clear paraboliclike streamlines distinguishing between regions of the jet flow and the cross flow on the upper wall, and that the induced velocity due to a pair of the vortex flow along the jet trajectory controls greatly streamlines on the upper wall. Several factors are pointed out to explain these behaviours of the streamlines.

## 1. Introduction

Gas turbine blades must operate in a high temperature environment to achieve a high thermal efficiency of gas turbine engines. This results in degradation of a blade material. Many kinds of blade cooling have been proposed to overcome the severe situation. One of them is the impingement cooling which is applied to the internal cooling of gas turbine vanes and blades by impingement means. Dealing with heat transfer problems on the impingement cooling, we need information on flow patterns and velocity and pressure distributions on the impingement surface, in addition to that on a jet trajectory, an impingement point and a vortex structure

in the cross-flow field affected by the impinging jet. Currently there are little or no experimental data on the flow pattern, velocity and pressure distributions on the impingement surface, as well the cross-flow field accompanied with the vortex structure.

Ref. 1) applied a finite-difference solution procedure to the problem of a round turbulent jet discharging at the right angle into a confined cross flow. The standard two-equation $k$-$\varepsilon$ model was used. The results agreed qualitatively with experiments, but improvement was necessary. Ref. 2) investigated experimentally effects of an opposite wall on jet trajectories and velocity and temperature distributions in cross planes and the symmetrical plane of the jet for unheated and heated jets, and for single and multiple jets. Ref. 3) obtained semianalytically jet trajectories and impingement points in confined, spatially variable cross flow on the basis of the three basic conservation equations and also their experimental results. Ref. 12) presented a semianalytical prediction of the trajectory of turbulent jets issuing at various angles to the horizontal into a crossflowing stream. This also dealt with trajectories of jets issuing into a cross flow with variable velocity and confined in a channel.

The references show that there are little aerodynamic data on the impingement cooling, notwithstanding the data are necessary to predict the heat transfer on the impingement wall.

In this situation of investigations on confined jets the authors investigate experimentally a three-dimensional flow generated by a jet issuing normal to a cross flow and impinging on an opposite wall of a channel. The present work is devoted primarily to studies of a vortex structure and a jet trajectory in a three-dimensional flow field and of an impinging flow pattern on the opposite wall. The present knowledge on the vortex structure and jet trajectories affected by it can be applied to a modelling analysis of the velocity field generated by the confined jet into a cross flow.

## Nomenclature

$C$ : magnitude of velocity vector $=|\boldsymbol{C}|=\sqrt{u^2+v^2+w^2}$
$C_e$ : effective cooling velocity acting on hot wire
$\boldsymbol{C}$ : velocity vector
$d$ : diameter of jet orifice $=20$ mm
$E$ : output voltage of hot wire
$h$ : height of channel
$k$ : yaw factor $=0.2$
$K$ : slope of linearized calibration curve for hot wire
$m$ : velocity ratio $=W_{jcenter}/U_\infty$
$u$, $v$, $w$ : velocity components (Fig. 4)
$U_\infty$ : main flow velocity
$W_j$ : local jet velocity
$W_{jcenter}$ : jet velocity at center of jet orifice
$x$, $y$, $z$ : cartesian coordinates with origin at center of jet orifice (Fig. 1)
$\gamma$ : pitch angle of velocity vector (Fig. 4)
$\lambda$ : angle between hot wire and $xy$ plane $=\pi/4$ (Fig. 4)

$\mu$ : roll angle of hot wire (Fig. 4)
$\xi$ : yaw angle of velocity vector (Fig. 4)
$\varphi$ : angle between velocity vector and hot wire (Fig. 4)

## 2. Apparatus and Procedure

Fig. 1 shows an arrangement of a working section, which has a rectangular cross section of 82 mm by 300 mm and a longitudinal length of 750 mm, and an air circuit for the jet, together with a probe used. The figure defines the channel coordinate system also. The working section used is mounted in a multipurpose working-section. Two bypasses are installed to remove a boundary layer developing on the tunnel floor upstream of the working section used. Accordingly a velocity distribution is uniform at the entrance of the working section, except in a boundary layer on its walls. There is the center of a 20 mm diameter jet orifice on the streamwise center-line of a flat channel floor, through which the jet issues normal to a cross flow. The thickness of the boundary layer on the channel floor, $\delta=[z]_{u=0.99U_\infty}$, is about 2 mm under no jet at $x/d=0$. Turbulence intensity in the working section is about 0.4% at $U_\infty=15$ m/s under no jet. Fig. 2 shows dimensions of a hot-wire probe with a sensor inclined at 45°. This probe, together with the I-type probe for a measurement near the upper wall, is mainly used. A sensing element is made of a 5 $\mu$m diameter tungsten wire, which is about 5.5 mm long and is plated with copper, except the central portion of 1mm long. The main flow velocity $U_\infty$ is 10.2 m/s under no jet at $x/d=0$ and the jet velocity at the center of the jet orifice, $W_{jcenter}$, is 36.6 m/s under no main flow. Thus $m$ is equal to 3.59. The present measurements are made only for $m=3.59$ in the range of $-1.175\leq x/d\leq 11.225$, $0\leq y/d\leq 4.2$ and $0.15\leq z/d\leq 4.1$. After output voltages of the hot wire $E_1$, $E_2$ and $E_3$, which correspond to three selected angles of $\mu$, are recorded on a pen recorder at every measuring point, their time-mean values are obtained graphically on the recorded data. They are employed to calculate $\gamma$, $\xi$ and $C$. Fig. 3 shows exit velocity profiles of the jet used.

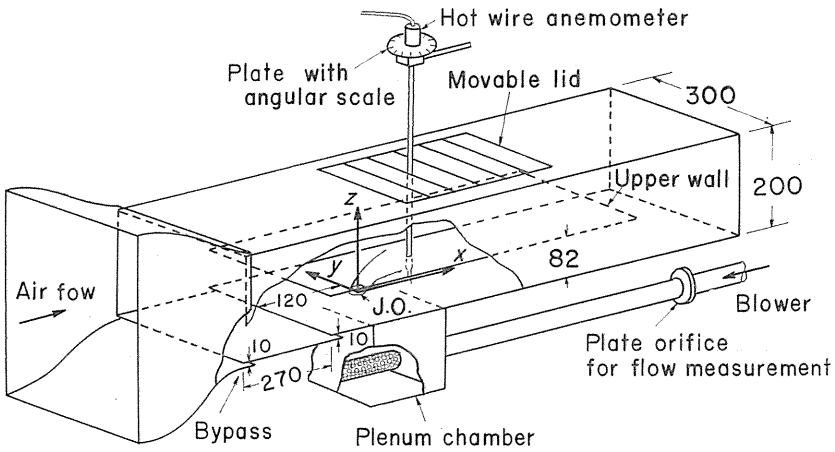


Fig. 1. Sketch of working section, showing notations. (J.O. Jet orifice)

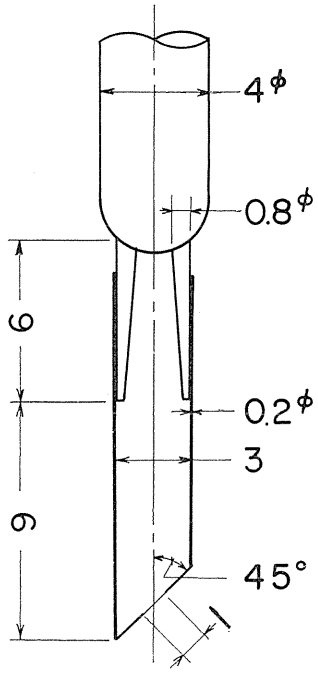


Fig. 2. Dimensions of inclined sensor hot wire probe used.

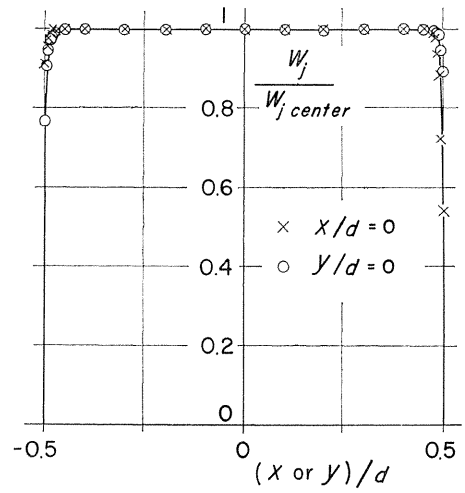


Fig. 3. Jet velocity profiles at jet exit. ($W_{icenter}$=36.6 m/s, $z/d$=0.05, $U_\infty$=0, $h/d$=0)

## 3. Data reduction

Several sources including Ref. 9) suggest that the effctive cooling velocity $C_e$ is expressed by

$$C_e=C\sqrt{1-(1-k^2)\cos^2\varphi} \tag{1}$$

for a hot wire in a free stream of velocity $C$. An electronic linearizer converts the nonlinear output of the hot wire into a linear form. Then $C_e$ is related to the output volage of the hot wire by the expression

$$E=KC_e=KC\sqrt{1-(1-k^2)\cos^2\varphi} \tag{2}$$

Referring to Fig. 4, we obtain the expression

$$\cos\varphi=\cos\lambda\cos\gamma\cos(\mu-\xi)+\sin\lambda\sin\gamma \tag{3}$$

Substituting Eq. (3) into Eq. (2), we have a hot wire response equation

$$E=KC\sqrt{1-(1-k^2)\{\cos\lambda\cos\gamma\cos(\mu-\xi)+\sin\lambda\sin\gamma\}^2} \tag{4}$$

We can solve Eq. (4) as a simultaneous equation with three unknowns $\xi$, $\gamma$ and $C$, because $\lambda$ is equal to $\pi/4$, if three output voltages of the hot wire are obtained at a measuring point in the flow field by changing the roll angle of the probe. When

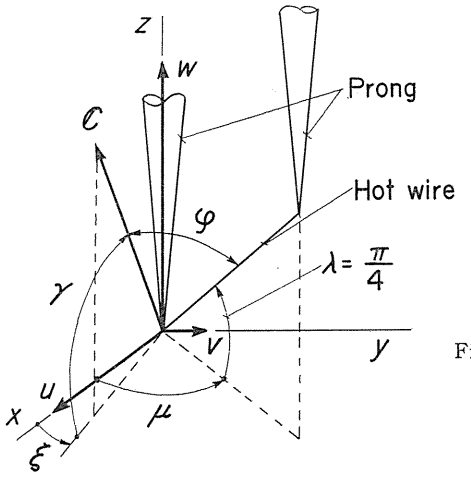


Fig. 4. Slanted hot-wire position and velocity vector related to coordinate reference system.

three roll angles, $\mu_1=\pi$, $\mu_2=3\pi/4$ and $\mu_3=\pi/2$, are selected, the unknown $\xi$ is given by the expression,

$$A\left\{\left(\frac{E_2}{E_1}\right)^2-1\right\}+\frac{1}{2}\left[\left(\frac{E_2}{E_1}\right)^2-1-\sqrt{1+\left(\frac{E_2}{E_1}\right)^4}\cdot\sin\left\{2\xi+\tan^{-1}\left(\frac{E_2}{E_1}\right)^2\right\}\right]\cdot\cos^2\left[\frac{1}{2}\left\{\sin^{-1}\frac{(M_1/2)-B}{\sqrt{M_2^2+(M_1/2)^2}}+\tan^{-1}\frac{M_1}{2M_2}\right\}\right]$$
$$+\left[\sin\left\{\sin^{-1}\frac{(M_1/2)-B}{\sqrt{M_2^2+(M_1/2)^2}}+\tan^{-1}\frac{M_1}{2M_2}\right\}\right]\cdot\sqrt{\frac{1}{2}+\left\{\left(\frac{E_2}{E_1}\right)^2-\frac{1}{\sqrt{2}}\right\}^2}$$
$$\cdot\sin\left[\xi+\tan^{-1}\left\{\sqrt{2}\left(\frac{E_2}{E_1}\right)^2-1\right\}\right]=0 \tag{5}$$

where $A=2/(1-k^2)-1=1.083$, $B=A\{(E_3/E_1)^2-1\}$, $M_1=\cos^2\xi-(E_3/E_1)^2\sin^2\xi$ and $M_2=\sin\xi+(E_3/E_1)^2\cos\xi$. A Newton iteration is used until the assumed and calculated values of $\xi$ are within one percent. If once $\xi$ is obtained, we can calculate immediately $\gamma$ and $C$ using the expressions,

$$\gamma=\frac{1}{2}\left[\sin^{-1}\frac{(M_1/2)-B}{\sqrt{M_2^2+(M_1/2)^2}}+\tan^{-1}\frac{M_1}{2M_2}\right], \tag{6}$$

$$C=\frac{\sqrt{2}E_1}{K}/\sqrt{(1-k^2)(A+\cos^2\gamma\sin^2\xi+\sin 2\gamma\cos\xi)} \tag{7}$$

At the flow field just above the jet orifice the following procedure is applied to calculate velocity vectors, because Eq. (5) solved by the Newton iteration does not give reasonable values of $\xi$. Eq. (3), together with $\lambda=\pi/4$, gives

$$\left.\begin{aligned}\cos\varphi_1&=(-\cos\gamma\cos\xi+\sin\gamma)/\sqrt{2}\\ \cos\varphi_2&=\left(\cos\gamma\cos\left(\frac{3}{4}\pi-\xi\right)+\sin\gamma\right)/\sqrt{2}\\ \cos\varphi_3&=(\cos\gamma\sin\xi+\sin\gamma)/\sqrt{2}\end{aligned}\right\} \tag{8}$$

for each of the above three selected roll angles $\mu_1$, $\mu_2$ and $\mu_3$. Substituting Eq. (2) into an equation obtained by eliminating $\xi$ from Eqs. (8), we have

$$\sin\gamma=\{\sqrt{2}\sqrt{1-(E_2/KC)^2}-\sqrt{1-(E_1/KC)^2}-\sqrt{1-(E_3/KC)^2}\}/\{(1-\sqrt{2})\sqrt{1-k^2}\} \tag{9}$$

Eq. (9) gives pitch angle $\gamma$ provided $C$ is assumed. Substituting Eq. (2) into an equation obtained by eliminating $\gamma$ from Eqs. (8), we have

$$\tan\xi=\frac{(1-\sqrt{2})\sqrt{1-(E_3/KC)^2}+\sqrt{2}\sqrt{1-(E_2/KC)^2}-\sqrt{1-(E_1/KC)^2}}{\sqrt{1-(E_3/KC)^2}-\sqrt{2}\sqrt{1-(E_2/KC)^2}+(\sqrt{2}-1)\sqrt{1-(E_1/KC)^2}} \tag{10}$$

Eq. (10) gives yaw angle $\xi$ provided $C$ is assumed. Eq. (10) becomes indeterminate, when $E_1$, $E_2$ and $E_3$ equal, namely $\gamma=\pi/2$. Using Eqs. (4), (9) and (10), together with $\lambda=\pi/4$, we can obtain $\gamma$, $\xi$ and $C$ using an iteration. The procedure is as follows. Substituting experimental values of $E_1$, $E_2$ and $E_3$ and $C^{[1]}$ as a first approximation of $C$ into Eqs. (9) and (10), we obtain $\gamma^{[1]}$ and $\xi^{[1]}$ which show first approximations of $\gamma$ and $\xi$, respectively. Then we can calculate a second approximation of $C$, namely $C^{[2]}$, for each value of $\mu$ using Eq. (4). An iteration is used until $C^{[1]}$ and $C^{[2]}$ are within one percent. If $C^{[1]}$ is equal to $C^{[2]}$ within an allowable error, we can determine a velocity vector by $C^{[1]}$, $\gamma^{[1]}$ and $\xi^{[1]}$.

## 4. Results and Discussion

### *4. 1. Velocity distributions on cross planes*

The left-hand side of Figs. 5 (a) to 5 (i) shows contours of $C$ in the regions upstream and downstream of the jet orifice. The right-hand side of Figs. 5 (a) to 5 (i) shows velocity vectors projected on cross planes.

The left-hand side of Figs. 5(a) and 5 (b) shows velocity contours upstream of the jet orifice. There is a region of decreasing velocity, in which the velocity contours spread upward like a fan. The decrease in velocity is due to a blockage effect of the jet on the cross flow. On the other hand, we find a region of increasing velocity near the lower wall at $x/d=-0.525$. The increase in velocity is attributed to an acceleration in stages that the cross flow near the lower wall goes around the jet flow, which has an aerodynamic effect similar to a solid cylinder, and that the cross flow is entrained into the jet through the region of the predominant negative pressure lying in the downstream region adjacent to the jet orifice. The right-hand side of Fig. 5 (b) indicates the flow into the region of the predominant negative pressure. The blockage effect of the confined jet on the cross flow is found in more upstream region than that of the unconfined jet. Refs. 1) and 2) do not indicate this. The left-hand side of Fig. 5 (c) shows the velocity contours including the jet region near the jet orifice. The right-hand side of it indicates generation of a vortexlike swirling flow. The left-hand side of Figs. 5 (d) and 5 (e) shows the velocity contours in the near downstream region of the jet orifice. We find the jet region bounded by a velocity contour with the kidney

shape. This jet region approaches to the upper wall with increasing $x/d$, as shown by the left-hand side of Figs. 5(c) to 5(f). The right-hand side of Figs. 5(d) and 5 (e) shows the vortexlike swirling flow coming into a flow region between the lower channel wall and the jet region with the kidneyshaped cross section and illustrates a process of development of the vortexlike flow, together with the right-hand side of Fig. 5 (c). The left-hand side of Fig. 5 (f) shows an example of kidneyshaped velocity contours, in which a single region of a high velocity is divided into two regions lying on both sides of the plane of symmetry. The swirling velocity near the lower wall is smaller at $x/d=2.25$ (the right-hand side of Fig. 5 (f)) than at $x/d=1.325$ (the right-hand side of Fig. 5 (e)), but the jet wake spreads laterally at $x/d=2.25$ more than at $x/d=1.325$ near the lower wall. The left-hand side of Figs. 5 (g) to 5 (i) shows velocity contours occurring after the jet has reached the upper wall. The left-hand side of Fig. 5 (h) includes a region of the maximum velocity ($C=12$ m/s) lying near the upper wall at a short distance from the plane of symmetry. We believe that this region comes from a lateral drift of the jet fluid due to the lateral velocity component induced by the vortexlike swirling flow, because there is a family of path lines spreading quickly laterally with increasing $x/d$ in the region of $x/d>5$ as shown later in Fig. 9 (a). In the region of $x/d\geq5.125$ the jet fluid flows along the upper wall and mixes quickly with the cross flow, because the velocity decreases markedly near the upper wall, as seen by the left-hand side of Fig. 5 (i). We can also find that the jet wake spreads laterally from $x/d=2.25$ to 5.125, as shown by the contours of $C=11$ m/s, and then reduces laterally with increasing $x/d$. The left-hand side of Fig. 5 (i) shows velocity contours in the region characterized by the vortexlike swirling flow. The decrease in velocity indicates that the mixing makes good progress between the jet and the cross flows in the whole cross plane.

The swirling flow governs the velocity distribution in the cross plane at $x/d\geq11.225$. From a magnitude of the swirling velocity vectors shown by the right-hand side of Figs. 5 (a) to 5 (i) the swirling flow develops up to $x/d\fallingdotseq3.275$ and then decays in the downstream region.

### *4. 2. Velocity distributions on the plane of symmetry and jet and vortex center-lines*

Figs. 6 (a) and 6 (b) show contours of the resultant velocity and its vector diagram, together with the jet center-line, in the plane of symmetry. The jet center-line is defined as the locus of the maximum velocity in the plane of symmetry. The stagnation streamline and the stagnation point on the upper wall are not found in the jet flow field in Figs. 6 (a) and 6 (b). This suggests that there is no reverse flow from an impingement area, because an impingement angle between the jet center-line and the upper wall is small in the present experiment. This phenomenon is easily explained by an analogy with a flow field produced by a two-dimensional jet impinging obliquely on a wall in no cross flow[10].

Ref. 2) also reports a velocity vector diagram, which is affected by a confined jet, in the plane of symmetry, but does not report it for a jet impinging on an upper wall. We find the following by comparison of Ref. 2) with the present experiment in the plane of symmetry. First it is pointed out that there is a region characterized by velocity vectors having a large pitch angle which means a strong entrainment into the jet (Fig. 6(b)). The region lies along and under the vortex center-line shown later in Fig. 7. The large pitch angle of the velocity

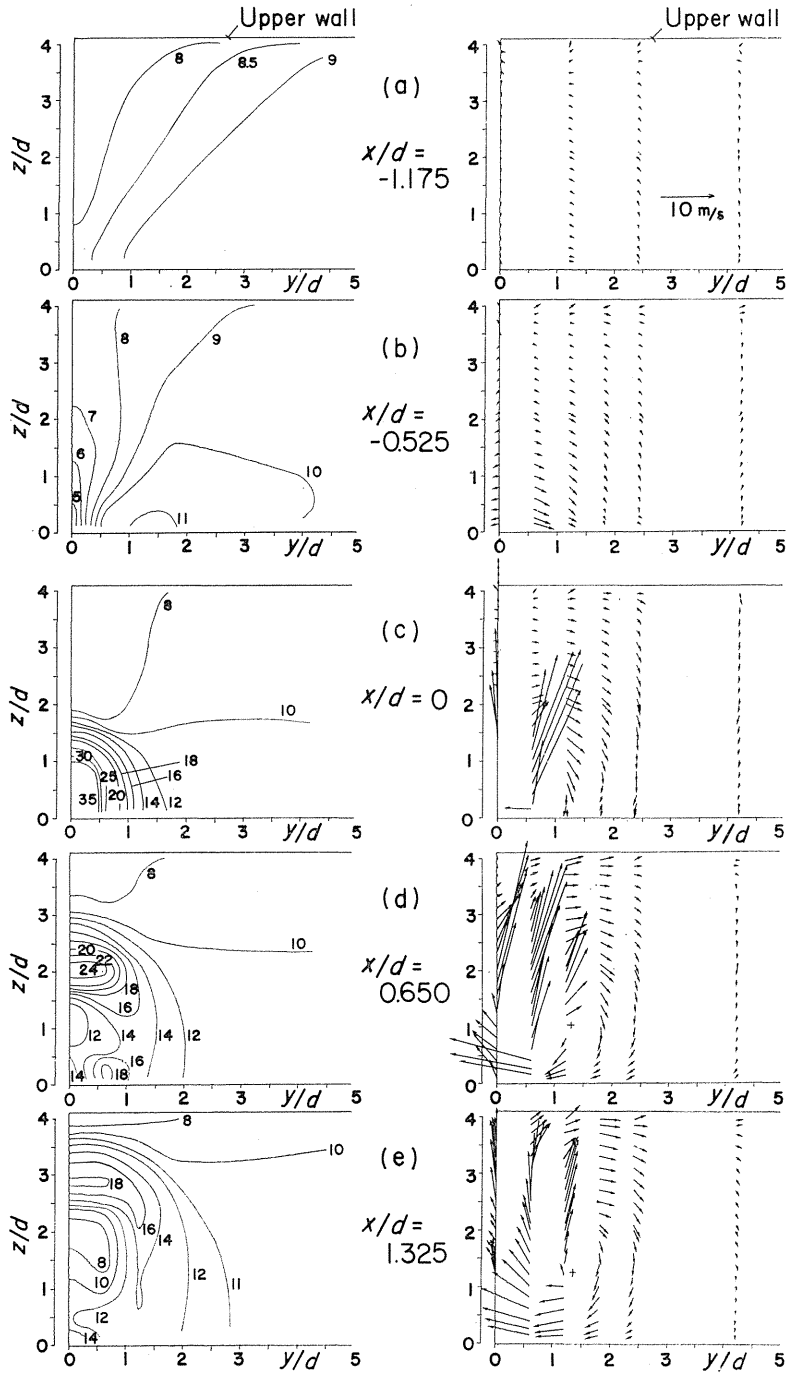


Fig. 5. Contours of $C$ (left-hand side) and projection of $\boldsymbol{C}$ (right-hand side) on planes normal to $x$ axis. (A symbol, +, expresses centers of the swirling flow. Numbers in the left-hand side of the figures indicate values of $C$ in m/s.)

vectors is due to an upwash induced by a pair of the swirling flows along the jet trajectory. This kind of the aerodynamic effect of the swirling flow is encountered later in Fig. 9 (a) also. Second it is indicated that the cross flow has a velocity component in the negative $z$ direction at $x/d=-1.175$ at least. This comes from a blockage of the cross flow due to the jet fluid impinging and accumulating on the upper wall.

Fig. 7 shows a comparison of the present experiments with the known empirical formulae for the jet and vortex center-lines. We see that the vortex center-line keeps the same position of $z/d$ in the downstream region of a point, where the jet

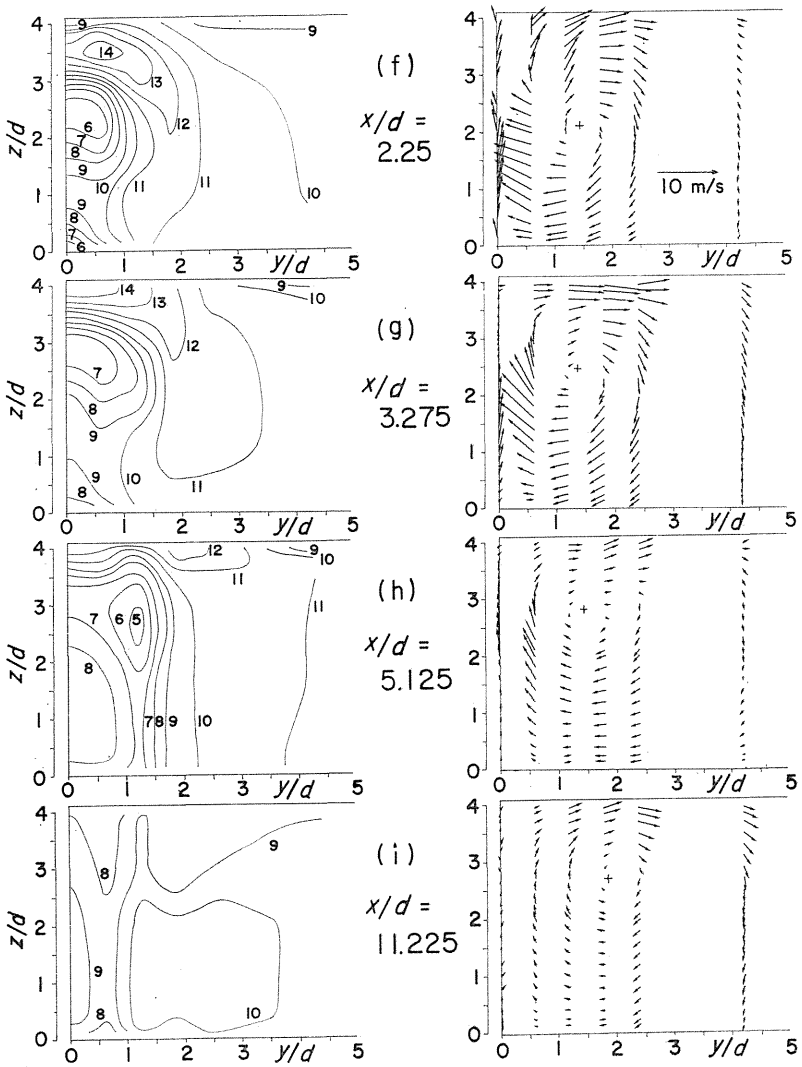


Fig. 5. Continued.

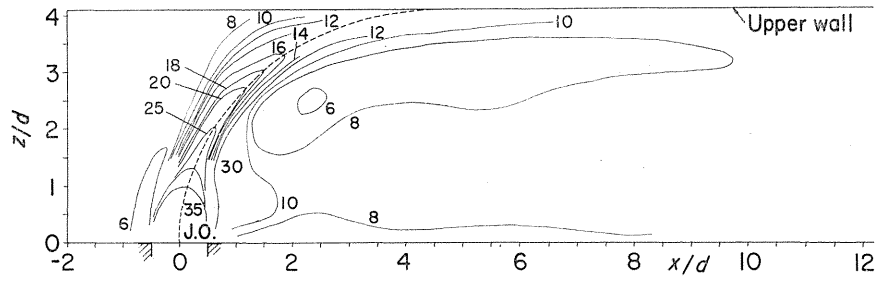


(a) Contours of $C$

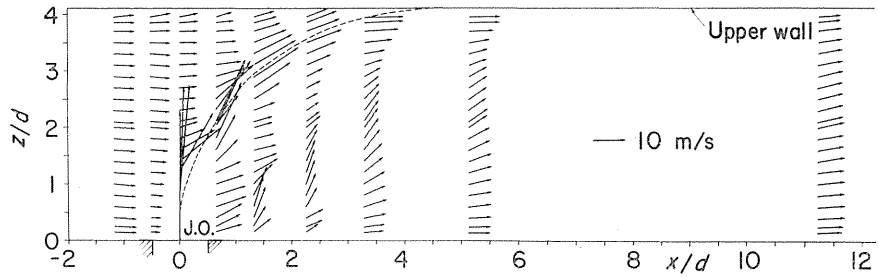


(b) Velocity vectors.

Fig. 6. Velocity distributions in plane of symmetry for jet. ($m=3.59$, $h/d=4.1$; ····· Jet center-line; J.O. Jet orifice; Numbers in the figure (a) indicate values of $C$ in m/s.)

center-line has almost reached the upper wall. The empirical formula[2) or 7)], which is shown by the curve ④ given by the equation ④ in the caption, deviates greatly from the present data. The empirical formula of the jet center-line in Ref. 2) or 7) is that for the unconfined jet, but it gives qualitatively a fairly good approximation to the present data, until the jet reaches the upper wall. As given in Ref. 2),

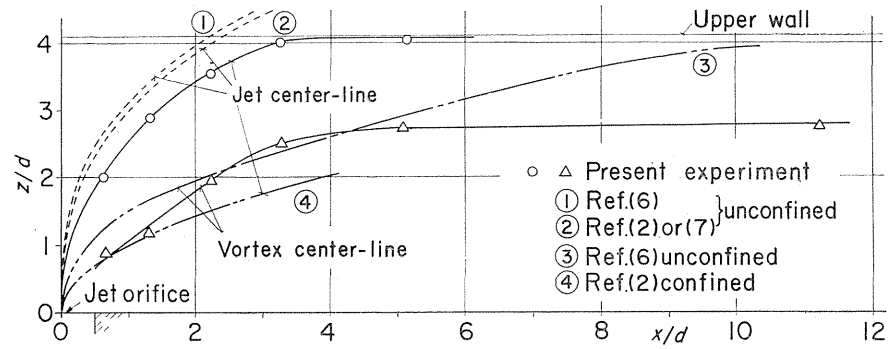


Fig. 7. Jet center-line, and vortex center-line projected on plane of symmetry for jet, together with empirical formulae for confined and unconfined jets plotted for comparison. ($m=3.59$, $h/d=4.1$; ① $z/d=0.9772m^{0.9113}(x/d)^{0.3346}$; ② $z/d=0.89m^{0.94}(x/d)^{0.36}$ for flat initial jet profile; ③ $z/d=0.3473m^{1.127}(x/d)^{0.4291}$; ④ $z/d=2.0m^{0.56}(x/d)^{0.5}(1-e^{-0.07(h/d)})$ for two-dimensional jet at $z<h/2$)

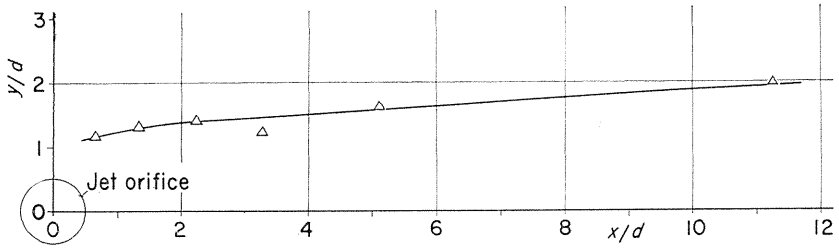


Fig. 8. Vortex center-line projected on $xy$ plane. ($m=3.59$, $h/d=4.1$)

using a constant 0.81 (for the fully developed initial profile) instead of 0.89 (for the flat initial profile) which is included in the expression for the curve ② (cf. the caption for Fig. 7), we can obtain a further good approximation to the present jet center-line. This means that when $m$ is as large as 3.59, the aerodynamic effects of the upper wall on the jet center-line are limited in the immediate neighbourhood of the upper wall.

Fig. 8 shows the vortex center-line projected on the lower wall. The vortex center-line is defined as a locus of the swirling center marked by the symbol, +, in the right-hand side of Figs. 5 (d) to 5 (i). The distance between the plane of symmetry and the vortex center-line projected is larger in the confined jet than in the unconfined one[6].

*4. 3. Oil flow patterns on the upper and lower walls*

Figs. 9 (a) and 9 (b) show an example of oil flow patterns on the upper and lower walls, respectively. It makes the accurate measurements near the upper wall difficult that the present experimental arrangement brings about a little leakage of the cross flow through a clearance between the sensor support and a hole for inserting it into the working section. In the situation a flow visualization technique is applied to discuss a flow field on the upper wall.

Fig. 9(a) shows that the jet fluid flows along the upper wall in the $y$ and positive $x$ directions, but there is no reverse flow in the impingement area of the jet. It is reasonable that the reverse flow generated by the jet fluid is assumed to be very small at the present velocity ratio $m=3.59$, as described in the discussion on Fig. 6. Thus we can see a pattern of a radial flow issuing from the region of $1.5<x/d<2$, $y/d=0$, but cannot see the reverse flow. There are two parabolic path-lines on both sides of the jet orifice projected on the upper wall. The downstream parabolic path-line of them corresponds to the upstream end of the region which keeps the predominant $z$ component of the jet velocity measured in the distance of 1mm below the upper wall. On the other hand, the upstream parabolic path-line of them corresponds to the upstream end of the region which keeps the predominant $y$ component of the jet velocity measured in the distance of 1mm below the upper wall. There is a family of path lines spreading laterally at a higher rate in the region of $x/d>5$. This comes from a pair of swirling flows which induce the upwash on the plane of symmetry. Exactly speaking, the upwash fluid branches off into two other streams in the $y$ direction after reaching the upper wall and separates laterally path lines from the plane of symmetry.

Fig. 9 (b) indicates that there is a V-shaped region ($0<x/d<2.5$) adjacent to the downstream end of the jet orifice. This forms a part of the flow path for the

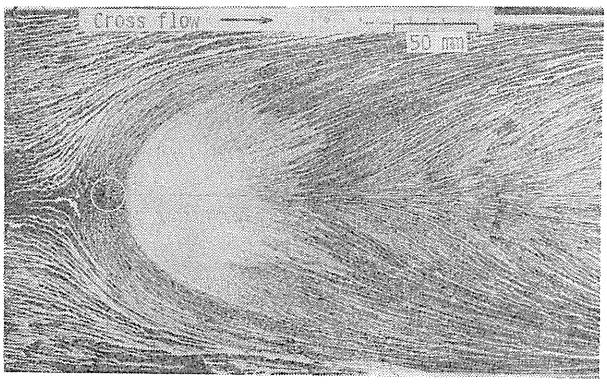


(a) Upper wall. (An open circle shows the jet orifice projected.)

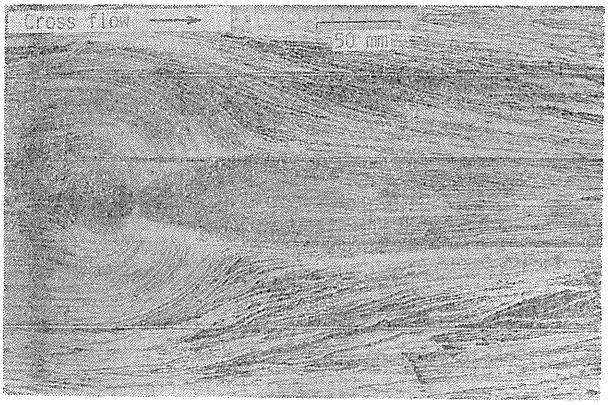


(b) Lower wall. (A closed circle shows the jet orifice.)

Fig. 9. Oil flow patterns. ($m$=3.59, $h/d$=4.1)

fluid entrained into the jet. Forms of the V-shaped region for the confined jet are similar to those for the unconfincd one, but an included angle of divergence of the V-shaped region is larger for the confined jet than for the unconfined one[11]. It is found that the included angle of divergence increases with increasing $m$ provided $h$ is fixed.

Several sources including Fig. 9 (b) suggest that there is another reverse flow due to the entrainment of the cross flow into the jet flow through the region near downstream of the jet orifice. Ref. 5) for an unconfined jet points out the reverse flow by illustrating an oil flow pattern in the plane of symmetry. Fig. 6 (b), however, suggests no sign of the reverse flow in the jet-wake region adjacent to the downstream end of the jet orifice. On the basis of this consideration further detailed measurements are necessary to confirm the reverse flow.

## 5. Conclusions

(1) When $m$ is as large as 3.59, aerodynamic effects of the upper wall on the jet center-line are limited in the immediate neighbourhood of the upper wall.

Thus the empirical formulae of the jet center-line for the unconfined jet[2) or 7)] can be used without a large error instead of that for the confined jet after some modification of a constant coefficient. On the basis of this the simple method in Ref. 3) is reasonable to determine the impingement point of the jet reaching the upper wall across a confined cross flow.

(2) The vortex center-line does not vary the position of $z/d$ after the jet center-line has reached the upper wall. The present vortex center-line is not predicted by empirical expressions obtained so far for the confined and unconfined jets.

(3) It is pointed out that there is the particular nature of oil flow patterns generated by the jet impinging on the upper wall. The mechanism of its generation is explained.

## Acknowledgments

The authors wish to acknowledge their indebtedness to Messrs. H. JIKEI and K. TATEZONO of the Department of Aeronautical Engineering for their kind help in experiments. This work was supported in part by the Grant-in-Aid for Scientific Research from the Japan Ministry of Education (No. 59550044, 1984; No. 61550045, 1986). The numerical calculations in this paper were carried out by the FACOM M-382 computer of Nagoya University.

## References

1) W. P. Jones and J. J. McGuirk: Computation of a Round Turbulent Jet Discharging into a Confined Cross-flow, Turbulent Shear Flow 2, eds L. J. S. Bradbury et al., Springer-Verlag (1980) pp. 233-245.
2) Y. Kamotani and I. Greber: Experiments on Confined Turbulent Jets in Cross Flow, NASA CR-2392 (1974).
3) R. L. Stoy and Y. Ben-Haim: Turbulent Jets in a Confined Crossflow, Trans. ASME, Journal of Fluids Engineering, Vol. 95, No. 4 (1973) pp. 551-556.
4) M. Inoue: Measuring Methods for Three-dimensional Flow Field by Hot-wire Technique, Turbomachinery, Vol. 10, No. 10 (1982) pp. 42-49, (in Japanese).
5) Y. Sugiyama and Y. Usami: Experiments on the Flow in and around Jets Directed Normal to a Cross Flow, Bulletin of the JSME, Vol. 22, No. 174 (1979) pp. 1736-1745.
6) R. Fearn and R. P. Weston: Vorticity Associated with a Jet in a Cross Flow, AIAA Journal, Vol. 12, No. 12 (1974) pp. 1666-1671.
7) Y. Kamotani and I. Greber: Experiments on a Turbulent Jet in a Cross Flow, AIAA Journal, Vol. 10, No. 11 (1972) pp. 1425-1429.
8) T. Ikui, et al.: Investigation on Measurements of Three-dimensional Turbulence by Multiscanning Mode for a Hot-wire Sensor, (1st Report, Measurements of Mean Velocity Vector), Preprint, Japan Soc. Mech. Engrs., No. 818-1 (1981) pp. 86-88, (in Japanese).
9) J. O. Hinze: Turbulence, 2nd ed., McGraw-Hill, (1975) p. 124.
10) W. Schach: Umlenkung eines freien Flüssigkeitsstrahles an einer ebenen Platte, Ingenieur-Archiv, Bd. V, Heft 4 (1934) pp. 245-265.
11) H. M. McMahon and D. K. Mosher: Experimental Investigation of Pressures Induced

on a Flat Plate, "Analysis of a Jet in a Subsonic Crosswind", NASA SP-218 (1969) pp. 49-62.

12) J. Sucec and W. W. Bowley: Prediction of the Trajectory of a Turbulent Jet Injected into a Crossflowing Stream, Trans. ASME, Journal of Fluids Engineering, Vol. 98, No. 4 (1976) pp. 667-673.